

HEARES 01249

A model for the peripheral auditory nervous system of the grassfrog

Ivo H.M. van Stokkum and C.C.A.M. Gielen

Department of Medical Physics and Biophysics, University of Nijmegen, The Netherlands

(Received 4 January 1989; accepted 7 May 1989)

A model is presented which incorporates several data from the literature on isolated parts of the peripheral auditory nervous system into a coherent model. The usefulness of the model lies in the fact that it describes the functional properties of eighth nerve fibres and dorsal medullary nucleus neurons in response to monaural stimuli.

The components are: a middle ear filter, transduction and tuning of the haircell, short-term adaptation, event generation with refractory properties, and coincidence detection. In a previous paper [Van Stokkum (1987), *Hear. Res.* 29, 223–235] a class of dorsal medullary nucleus neurons was described, which preferred fast intensity changes. Using a coincidence detection mechanism the proposed model reproduces the same preference. Variation of the parameters of the model successfully reproduces the range of response patterns which have been obtained from eighth nerve fibres and dorsal medullary nucleus neurons. With one set of parameters the output of the model in response to a set of spectrally and temporally structured stimuli qualitatively resembles the response of a single neuron. In this way the responses to the different stimuli are synthesized into a framework, which functionally describes the neuron.

Anuran; Auditory nerve; Coincidence detection; Dorsal medullary nucleus; Neural modeling; Temporal selectivity

Introduction

For almost three decades the anuran auditory system has been studied with electrophysiological methods (for reviews see Fritzsche et al., 1988). Thereby much work has been devoted to the exploration of single-unit characteristics. In these studies parameters of a sound stimulus were varied, and the response of a neuron was recorded extracellularly. A selective response of a neuron to a certain range of parameters is then supposed to be related to the function of this neuron in the processing of sound. Large quantities of single-unit

data have been gathered and interpreted. However, this interpretation has not yet led to a mathematical description in terms of a coherent model, which explains the response characteristics of neurons to a wide class of stimuli. In this paper we present a quantitative model, which simulates the responses of eighth nerve fibres and dorsal medullary nucleus neurons. DMN neurons are innervated chiefly by fibres from the ipsilateral NVIII and the contralateral DMN (Feng, 1986).

The natural calls of the grassfrog and of several other anurans consist of trains of pulses. For the identification of these calls several cues are available, such as spectral content, pulse shape, pulse repetition rate, and slow pulse amplitude modulation. Many authors (e.g. Gerhardt and Doherty, 1988) have shown that these and other cues are actually used in female mate choice. In contrast, many electrophysiological studies have been limited to a single class of stimuli, exploring the selectivity for either frequency or amplitude modulation. In a foregoing paper (Van Stokkum, 1987) we have investigated neurons in the DMN of the

Correspondence to: Ivo H.M. van Stokkum, Department of Medical Physics and Biophysics, University of Nijmegen, P.O. Box 9101, 6525 EZ Nijmegen, The Netherlands.

Abbreviations: AMF, amplitude modulation frequency; AP, whole nerve action potential; CF, characteristic frequency; DMN, dorsal medullary nucleus; EPSP, excitatory postsynaptic potential; F_c , centre frequency; NVIII, eighth nerve; PRR, pulse repetition rate; SNR, signal-to-noise ratio; SPL, sound pressure level.

grassfrog, using an ensemble of stimuli with spectral as well as temporal parameter variation. It is our belief that the use of a broad ensemble of stimuli will provide more insight into the underlying mechanisms which are responsible for the observed neural selectivities. Therefore we developed a model which incorporates spectral as well as temporal aspects of signal processing. Thereby our attention was focused upon neural mechanisms, whereas less attention was paid to the precise origin of the frequency selectivity, which constitutes a research area in itself. Our model consists of a system-theoretical description of frequency selectivity, adaptation, event generation in the NVIII, and coincidence detection in the DMN. In this paper the model is restricted to monaural stimuli. The results of the model simulations will be compared to experimental data described in the literature (NVIII and DMN) or obtained in our lab (DMN).

Methods

Single unit recordings were made in the DMN of the immobilized grassfrog. The sound stimulus was presented ipsilaterally through a closed sound system. The frog's mouth was kept open during the experiment, in order to decouple both ears (Vlaming et al., 1984). A detailed description of the recording and sound stimulation methods has been given before (Van Stokkum, 1987).

Components of the model

Middle ear

The transfer of the sound pressure stimulus from the coupler to the inner ear is described by an impulse response $h(t)$, which is shown in Fig. 1A. Based on measurements of the amplitude and phase of the tympanum displacement as a function of frequency (Vlaming et al., 1984) Aertsen et al. (1986) have modeled the auditory periphery. Departing from their model we have derived the impulse response of the middle ear:

$$h(t) = 2\gamma e^{-\gamma t} \sin(\omega_1 t) \Theta(t) \quad (1)$$

with $\Theta(t) = 1$ if $t > 0$, and $\Theta(t) = 0$ if $t \leq 0$. The

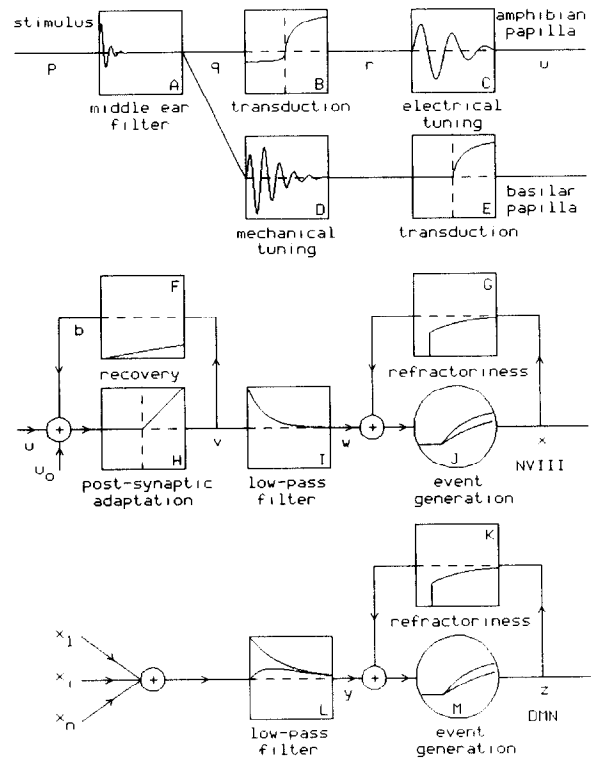


Fig. 1. Model for the processing of sound by the amphibian and basilar papilla, NVIII and DMN of the grassfrog. The stimulus waveform is band-pass filtered by the middle ear (Fig. 1A), and filtered and transduced into a haircell potential (Figs. 1B and C for the amphibian papilla, Figs. 1D and E for the basilar papilla). The synapse between the haircell and the dendrite of the NVIII comprises of a short-term adaptation mechanism (Figs. 1F and 1H) and a low-pass filter (Fig. 1I). From the generator potential w of the NVIII fibre action potentials are generated (Fig. 1J), which form the point process x . Absolute and relative refractory mechanisms are incorporated in the negative feedback (Fig. 1G). Several NVIII fibres converge upon a DMN neuron, where they add linearly. From the generator potential y of the DMN neuron action potentials are generated in the same way as above. In Figs. 1A,C,D,F,G,I,K and L impulse responses are drawn on a timebase of 5 ms. Figs. 1B,E and H represent the instantaneous nonlinearities of Eqs. 2, 4 and 5. Figs. 1J,M show the probability of event generation (Eqs. 12, 13) as function of the generator potentials w, y . Further explanation in text.

parameters ω_1 , the middle ear resonance frequency, and γ , the decay rate, are put equal to, respectively, $2\pi \cdot 0.876$ kHz, and 1.297 (ms) $^{-1}$. This description of the middle ear response is valid up to about 1.5 kHz (Vlaming et al., 1984).

Mechano-electrical transduction and tuning

Anurans possess two separate auditory receptors, the amphibian and the basilar papilla. The tuning mechanism is different for each papilla (for review see Zakon and Wilczynski, 1988). The tuning of the amphibian papilla is in part due to an active process, which is metabolically vulnerable. The basilar papilla is thought to be tuned only mechanically. In Figs. 1B–E the model is drawn in parallel for haircells of the amphibian and basilar papilla.

The response of a haircell to mechanical stimulation of its stereocilia is nonlinear, showing rectification and saturation (Hudspeth, 1983). Following Crawford and Fettiplace (1981b) this is modeled with a function shown in Fig. 1B:

$$r(q) = \frac{q}{q + q^0} \Theta(q) + \frac{q}{q^0 - \rho q} \Theta(-q) \quad (2)$$

In the turtle Crawford and Fettiplace measured a mean half-saturation sound pressure q^0 of 86 dB SPL, and a mean ρ , the ratio of maximum increase and decrease, of 4. The saturation at higher sound pressure levels models well known nonlinear phenomena like two-tone suppression and difference-tone excitation (Capranica and Moffat, 1980). This way of modeling two-tone suppression has also been proposed by Crawford and Fettiplace (1981b). The cascade linear filter – nonlinearity – linear filter, in systems theory known as a sandwich system, has been used before by Johannesma (1971) to model frequency selectivity.

Pitchford and Ashmore (1987) demonstrated electrical resonance in haircells of the amphibian papilla. The membrane potential showed oscillations, the frequency of which varied in accordance with the tonotopical organization of the amphibian papilla. In the rostral part of the amphibian papilla they measured resonance frequencies between 0.06 and 0.33 kHz. Furthermore Whitehead et al. (1986) measured otoacoustic emissions with frequencies between 0.5 and 1.0 kHz. These may originate from haircell membrane oscillations in the caudal part of the amphibian papilla. The frequency tuning of the haircell membrane is described by a band-pass filter with impulse response $f_i(t)$:

$$f_i(t) = 2\beta_i^{-2} t e^{-t/\beta_i} \sin(\omega_i t) \Theta(t) \quad (3)$$

The time-constant β_i determines the sharpness of the filter, and ω_i is equal to $2\pi \cdot F_c$, the centre frequency. The characteristic frequencies of NVIII fibres innervating the amphibian papilla range from 0.1 to 1.0 kHz. An example of an impulse response $f_i(t)$ is shown in Fig. 1C. Such an impulse response is called a gammatone (Aertsen and Johannesma, 1980). Van Gisbergen et al. (1975) showed that the frequency selectivity of low frequency cochlear nucleus neurons in the cat as determined with noise stimuli could be adequately described with gammatone impulse responses (see also De Boer and Kuyper, 1968).

The mechanical tuning of the basilar papilla is also modeled with a filter $f_i(t)$ (see Fig. 1D). The characteristic frequency of NVIII fibres innervating the basilar papilla is between 1 and 1.5 kHz for the grassfrog (Schneider-Lowitz, 1983). For the basilar papilla the mechano-electrical transduction follows the mechanical filter, and a function like $r(q)$ (Eq. 2) would generate no output in its linear range, when followed by the low-pass filter of the haircell membrane. We assume that the dynamical characteristics of the transduction cause a rectification. The transduction is modeled with $u(r)$, shown in Fig. 1E:

$$u(r) = \frac{r}{r + r^0} \Theta(r) \quad (4)$$

Adaptation

Megela and Capranica (1981) have demonstrated a diversity of short-term adaptation patterns in the anuran auditory nerve. The basilar papilla fibres show more or less the same modest adaptation to 750 ms tonebursts. Fibres innervating the amphibian papilla showed response patterns ranging from tonic to phasic, which in some cases depended upon carrier frequency or intensity (Megela, 1984).

The short-term adaptation component is basically a half-linear high-pass filter. It is a simplified version of the model of Eggermont (1985), who ascribed adaptation to postsynaptic processes. The input is provided by a transmitter release proportional to u plus u_0 , where u_0 is the spontaneous

release. There is only release when $u + u_0$ is positive. The transmitter occupies postsynaptic receptors giving rise to an output v , proportional to the number of active receptors. The receptors are inactivated with rate λ . The inactivated receptors ($-b$) recover with rate μ . Note that b is a negative quantity, which is added to u plus u_0 . The adaptation component is described by the following equations:

$$v = (u + u_0 + b)\Theta(u + u_0 + b) \quad (5)$$

$$\frac{db}{dt} = -\lambda v - \mu b \quad (6)$$

The differential equation for b corresponds with a first-order low-pass filter, with time-constant μ^{-1} (see Fig. 1F). When $u_0 = 0$, multiplication of input u with α results in multiplication of the output v with α , a consequence of the halflinearity of the rectifier (Fig. 1H). Note that omission of the rectifier would leave us with a high-pass filter.

Phase-locking

Auditory nerve fibres show phase-locking which declines with increasing frequency. Hillery and Narins (1987) found phase-locking up to 900 Hz. A possible explanation for the decline of phase-locking is the low-pass filtering by the haircell membrane, demonstrated in the guinea-pig by Palmer and Russell (1986). Low-pass filtering is also performed postsynaptically in the form of excitatory postsynaptic potentials. Crawford and Fettiplace (1980) measured a decay time-constant of 1 ms for the EPSPs, in the turtle, at room temperature. The decline of phase-lock is modeled with a first-order low-pass filter $l(t)$ (see Fig. 1I):

$$l(t) = \omega_2 e^{-\omega_2 t} \Theta(t) \quad (7)$$

Parameter ω_2 determines the cut-off frequency for phase-locking, and is put equal to 1 (ms)^{-1} .

Event generation

The generation of action potentials (events) is a stochastic process and is modeled with help of a generator function $g(w)$, known in point process literature (e.g. Cox and Isham, 1980) as the inten-

sity function. The probability of event generation in an interval dt is:

$$P[N(t+dt) - N(t) = 1] \\ = g(w(t); N(s), s < t) dt \quad (8)$$

Here $N(t)$ is the counting process, which represents the number of events up to time t . Thus $N(t)$ is the integral of the generated point process $x(t)$ (e.g. Cox and Isham, 1980). The argument of the generator function depends in two ways on the events generated in the past. Firstly, after an event has been generated the probability per unit of time to generate an event, $g(w)$, is zero for an absolute refractory period τ_{abs} . Secondly, to model relative refractoriness a negative feedback is supplied to the event generator. This feedback is given by the impulse response $c(t)$, which starts after the end of τ_{abs} :

$$c(t) = -R e^{-(t-\tau_{abs})/\tau_R} \Theta(t - \tau_{abs}) \quad (9)$$

The refractory mechanism is illustrated in Figs. 1G and 1K, with $\tau_{abs} = 1 \text{ ms}$ and $\tau_R = 2 \text{ ms}$. In a simulation with binwidth Δt the function $g(w)$ is constant within a single bin. When $\Delta t < \tau_{abs}$ at most one event can be generated in a single bin and we have:

$$P[\Delta N(t) = 1] + P[\Delta N(t) = 0] = 1 \quad (10)$$

Here $\Delta N(t) = N(t + \Delta t) - N(t)$. Suppose we divide the bin Δt in n parts, and let n go to infinity. Then the probability of zero events in the interval Δt becomes:

$$P[\Delta N(t) = 0] = \lim_{n \rightarrow \infty} \left(1 - \frac{g(w)\Delta t}{n}\right)^n = e^{-g(w)\Delta t} \quad (11)$$

Combining Eqs. 10 and 11 we get:

$$P[\Delta N(t) = 1] = 1 - e^{-g(w)\Delta t} \quad (12)$$

For the generator function $g(w)$ any non-negative function can be chosen. We have used a half-linear function:

$$g(w) = v(w - m)\Theta(w - m) \quad (13)$$

For w less than m , the threshold parameter, $g(w)$ is zero. As a consequence, when m is positive, spontaneous activity can only be generated with a positive generator potential. Parameter ν determines the slope of $g(w)$. In Fig. 1J and M the probability of event generation according to Eqs. 12 and 13 is drawn for two different values of ν .

Convergence of inputs

We assume that there is a convergence of many NVIII fibres upon a single DMN neuron. Based upon Rall's model (1977) of neuronal cable properties, convergence of inputs is modeled as linear summation of the input point processes, which are then low-pass filtered to arrive at compound EPSP's. In formula (Johannesma and Van den Boogaard, 1985):

$$y(t) = \sum_{i=1}^n \int ds e_i(s) x_i(t-s) \quad (14)$$

with

$$e_i(t) = W e^{-t/\tau_d} (1 - e^{-t/\tau_u}) \Theta(t) \quad (15)$$

Here $x_i(t) = \sum_{j=1}^{N_i} \delta(t - t_{i,j})$ represents the events

at times $t_{i,j}$ of NVIII fibre i . In Fig. 1L two different EPSP shapes $e_i(t)$ are drawn. In our simulations we have chosen an EPSP with rise and decay time-constants of, respectively, 0 and 1 ms.

Implementation of the model

The model was programmed in Fortran 77 on a VAX 11/785 computer. Stimuli which were used for single unit recording from auditory neurons were sampled and provided the input to the model. The sample interval usually was 0.1 ms, but for lengthy stimuli it was 0.2 or 0.25 ms.

A summary of the parameters used in the main simulations of this paper is given in Table I. The degrees of freedom are: the amount of nonlinearity in the transduction, the tuning characteristics, the short-term adaptation and recovery time-constants, and, most important, the parameters which determine the event generation and refractory properties.

Outputs of the model are the generator potentials w and y , and the time-series x and z , which mimic the occurrences of action potentials in, respectively, a NVIII fibre or a DMN neuron. The generator potentials help to understand the action of the several nonlinearities incorporated in the model. The time-series x and z , or averages thereof

Table I
MODEL PARAMETERS

Parameters	Eq.	Related to	Value
γ, ω_1	1	middle ear filter	$1.297 \text{ (ms)}^{-1}, 2\pi \cdot 0.876 \text{ kHz}^a$
ρ	2	transduction asymmetry	4^b
q^0, r^0	2,4	transduction saturation	1
ω_i, β_i	3	tuning characteristics	variable
u_0	5	spontaneous activity	0
λ^{-1}, μ^{-1}	6	short-term adaptation	5 ms, 1000 ms
ω_2	7	dendritic low-pass filter	1 (ms)^{-1c}
$\tau_{\text{abs}}, R, \tau_R$	9	refractory properties	NVIII: 4–5 ms, 0.05, 2 ms DMN: 6 ms, 1.2, 2 ms
m, ν	13	event generation	NVIII: $0.0003\text{--}0.003, 250 \text{ (ms)}^{-1}$ DMN: $0.45, 10 \text{ (ms)}^{-1}$
n	14	amount of convergence	16
W	15	EPSP height	0.1
τ_d, τ_u	15	EPSP shape time delay	1 ms, 0 ms NVIII \rightarrow DMN: 2 ms

^a derived from Aertsen et al. (1986), p. 21, 25.

^b Crawford and Fettiplace (1981b), p. 326.

^c Crawford and Fettiplace (1980), p. 91.

in the form of histograms, are directly compared to experimental data obtained in the NVIII and the DMN, described in the literature or obtained in our lab.

Results

Frequency tuning

The frequency tuning of the model will be illustrated with plots of isopotential contours of the generator potential w . These are comparable to frequency tuning-curves as measured in the NVIII.

In Fig. 2 filter properties and tuning characteristics are illustrated. Columns one and two show, respectively, the impulse response and power-spectrum of filters with centre frequencies of 1.25, 0.625 and 0.2 kHz and of the middle ear filter. In the third column isopotential contours are shown. The carrier frequency of the tonepips varies horizontally, the intensity vertically, both on a logarithmic scale. The intensity varies from -40 to $+20$ dB relative to the half-saturation point q^0 , respectively r^0 (see Eqs. 2 and 4). From top to bottom tuning is visible with the centre frequency approximately equal to that of the filter. The main parameter responsible for the tuning quality is β . A larger β means a longer impulse response and a sharper tuning.

Two-tone suppression

The consequences of the different order of band-pass filter and nonlinearity in Figs. 1B,C and 1D,E are demonstrated with a two-tone stimulus. A second tonepip with an intensity of -20 dB relative to q^0 or r^0 and a carrier frequency equal to the F_c of the filter was added to the tonepip stimulus. The isopotential contours are shown in the fourth column of Fig. 2. Suppression of the response to the second tonepip is visible for both amphibian papilla filters. In particular, the area indicated by the minus sign in the $F_c = 0.2$ kHz box is comparable to a suppression tuning curve as shown in Fig. 11 of Capranica and Mofat (1980). The suppression can be understood as follows: a high intensity tone away from F_c drives the nonlinearity (Eq. 2, Fig. 1B) in the saturation

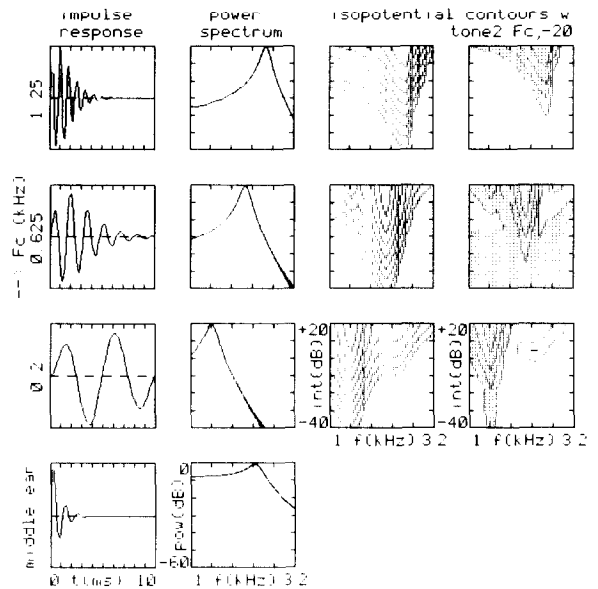


Fig. 2. Characteristics of the filters and of the generator potential w for three sets of parameters. *Column one*: first 10 ms of impulse response of filter. *Column two*: power spectrum on a logarithmic scale from 0.1 to 3.2 kHz. *Column three*: isopotential contours of the generator potential w obtained with tonepip stimuli. The carrier frequency varied logarithmically between 0.1 and 3.2 kHz, the intensity between -40 and $+20$ dB relative to q^0 or r^0 . Adaptation was left out of the model. The difference between two isopotential contours is a factor two. *Column four*: isopotential contours of w obtained with two-tone stimuli. A second tonepip at the centre frequency of the filter and at an intensity of -20 dB relative to q^0 or r^0 was added to the stimulus of column three. The shading represents values higher than the maximum divided by 16. The minus sign in row three represents values below the maximum divided by 32. *Row one*: Basilar papilla haircell, $F_c = 1.25$ kHz, $\beta = 0.8$ ms, see Eq. 3. *Row two*: Amphibian papilla haircell, $F_c = 0.625$ kHz, $\beta = 1.5$ ms. *Row three*: Amphibian papilla haircell, $F_c = 0.2$ kHz, $\beta = 4.0$ ms. *Row four*: middle ear, see Eq. 1.

range which results in a signal compression. Thus the second tone at F_c is compressed by the nonlinearity, resulting in a suppression of the haircell potential u and generator potential w . In the basilar papilla branch of the model a high intensity tone away from F_c will simply be filtered out (Fig. 1D).

Adaptation and masking

According to Eggermont (1985) short-term adaptation and forward masking are interrelated

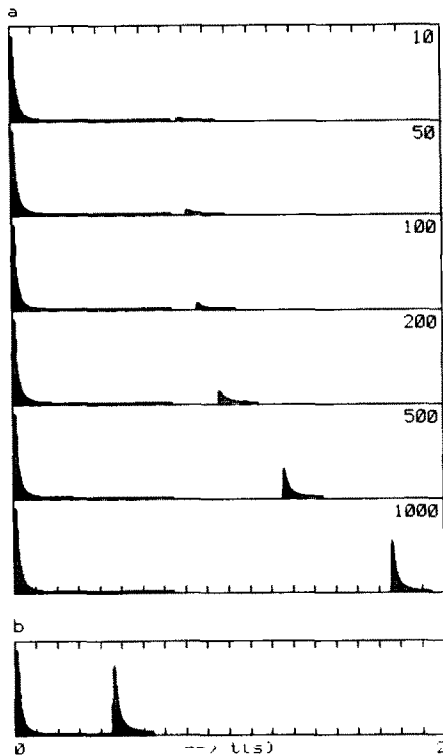


Fig. 3. Simulation of forward and simultaneous masking. (a) In the forward masking paradigm of Megela and Capranica (1982) a masking tone of 750 ms is followed after an interval by a test tone of 200 ms. The intervals are indicated at the right. The generator potential w is plotted on a timebase of 2 s. (b) In the simultaneous masking paradigm the test tone was started 450 ms after the onset of the masking tone.

phenomena. In his model (see also Eqs. 5 and 6) the short-term adaptation and the forward masking time-constants are, respectively, $(\mu + \lambda)^{-1}$ and μ^{-1} . The relative steady state firing rate is $\mu/(\mu + \lambda)$. This interrelation is supported by the experiments of Megela and Capranica (1982), who found that masking was strongest (μ^{-1} large) for fast-adapting amphibian papilla fibres (λ large, $\mu/(\mu + \lambda)$ small).

A forward masking experiment following the protocol of Megela and Capranica was simulated. In their experiments a masking tone of 750 ms was followed by a test tone of 200 ms, after an interval which varied between 10 and 1000 ms. Fig. 3a shows the generator potential w as a function of time. First there is adaptation to the 750 ms masking tone. The peak of the response to

the test tone is negligible just after the offset of the masker, but almost recovers within 1 s, in accordance with the recovery time-constant μ^{-1} , which is 1 s in this simulation. As an extension simultaneous masking is illustrated in Fig. 3b, where a test tone was presented during the masking tone, starting at 450 ms after the onset of the masker. The increment response is similar to the onset response to the masker. Note that after the end of the test tone the response to the masker is totally suppressed.

Response to temporally structured stimuli

In the NVIII Rose and Capranica (1985) found no selectivity for amplitude modulation frequency (AMF) with respect to firing rate. However, with respect to synchronization to the envelope, they found low-pass characteristics for fibres innervating the amphibian papilla. Basilar papilla fibres showed increased synchronization to AMFs between 100 and 150 Hz. This is in accordance with the findings of Hillery (1984), who reported a larger AP with these AMFs, using a carrier frequency of 2 kHz. The AP presumably results from synchronized activity of NVIII fibres.

Schneider-Lowitz (1983) studied the responses to trains of 10 ms pulses, with a duration of 500 ms and a pulse repetition rate varying between 5 and 100 Hz, in the NVIII and in the DMN. With respect to firing rate all NVIII fibres increased their response with increasing PRR, until they reached a saturation level at PRRs between 35 and 100 Hz. In the DMN only 28% showed the same behavior, the other neurons showed a decline of the rate response above a PRR between 10 and 60 Hz.

DMN units showing a strong preference for fast intensity changes were reported by Van Stokkum (1987). This is illustrated by the responses of unit 297,0,6 in Fig. 4, a unit which was already described elaborately in Van Stokkum (1987). The frequency selectivity parameters of the unit are: threshold just below 80 dB peak SPL, CF 0.63 kHz. In Figs. 4a and 4b the response to pulse shape variations, at stimulus intensities of, respectively, 80 and 90 dB peak SPL, is shown in the form of a reordered eventdisplay along with a spike rate histogram. In this paper spike rate is

defined as the average number of action potentials per stimulus presentation. The action potentials in response to the 20 presentations of a pulse shape are drawn one underneath the other as dots. From top to bottom the stimulus consists of a click (c), a pulse from the mating call (*), a time-reversed pulse from the mating call (r*), tonepips (p) with a duration of 5, 10, 20, and 50 ms, and tonepips of 10, 20, and 50 ms with a gamma-envelope (Γ) (Aertsen and Johannesma, 1980), alternated by their time-reversed versions (r Γ). Rise and fall times of the different pulse shapes are: 0.1 ms (c), 2 and 10 ms (*), 10 and 2 ms (r*), 1 ms (p), 20% and 80% of the duration (Γ), and 80% and 20% of the duration (r Γ). The carrier frequency for the tonepips is 0.63 kHz. A remarkable finding is that this unit has a lower threshold for pulse shapes with a fast rise time and a slow fall time (* and Γ) than for their time-reversed versions. Unit 297,0,6 does not respond to r Γ 50 at either intensity. The response to r* changes both in rate and latency. In response to r Γ 20 only two action potentials are seen at 90 dB.

The second stimulus (Figs. 4c and 4d) consists of amplitude-modulated tonebursts (Epping and Eggermont, 1986) of 500 ms, with overall rise and fall times of 100 ms, a carrier frequency of 0.63 kHz, and stimulus intensities of, respectively, 80 and 90 dB peak SPL. At the bottom line responses to an unmodulated toneburst are depicted. The AMF of the other tonebursts varied logarithmically between 7.8 and 250 Hz (top). Unit 297,0,6 responds to AMFs between 62 and 125 Hz during the rise time of the toneburst. The response is about twice as strong at 90 dB. To click trains with a pulse repetition rate varying from 7.8 to 250 Hz (Fig. 4e) the unit responds in a time-locked fashion to each click up to a PRR of 62 Hz. With higher PRR the response deteriorates, until at 250 Hz only one action potential is left at the onset. This low-pass character of the rate response corresponds well with the findings of Schneider-Lowitz (1983) mentioned above.

The mating call of the grassfrog consists of a series of pulses with a PRR of about 36 Hz and a slowly increasing pulse amplitude. The energy in a pulse is concentrated at frequencies near 0.55 kHz. The stimulus of Fig. 4f consists of mating calls (*), and time-reversed mating calls (r*), against

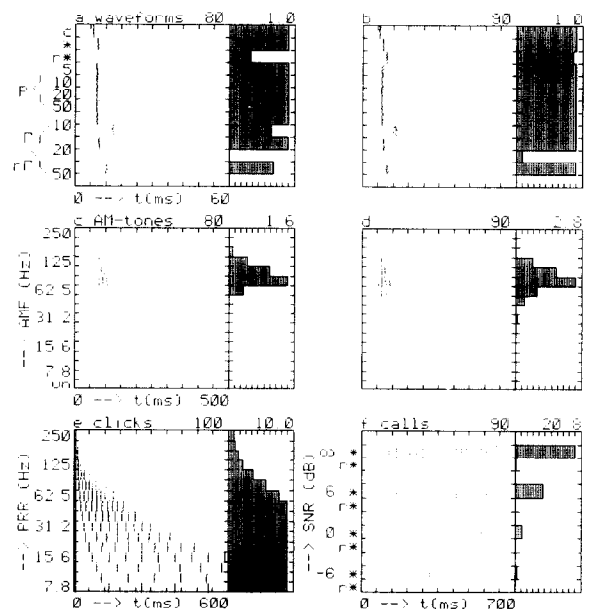


Fig. 4. Reordered eventdisplays together with rate histograms of responses of DMN unit 297,0,6 to six different stimuli. At the left the stimulus parameter variation is indicated. All stimuli were presented ipsilaterally. The intensities, in dB peak SPL, are indicated above each eventdisplay. Carrier frequency in (a–d) 0.63 kHz. Above each histogram the maximum value is written. Note the different timebases, which are indicated under the eventdisplays. The different stimulus waveforms in Figs. a and b were: click (c), pulse from the mating call (*), tonepip (p), gammatone (Γ), and time-reversed versions (r* and r Γ). The durations of the tonepips and of the gammatones are indicated. The AMF of the tonebursts (c and d) varied between 7.8 and 250 Hz, in addition an unmodulated toneburst (un) was presented. The equidistant click trains of (e) consisted of 10 clicks with PRR varying between 7.8 and 250 Hz. The mating call (*) and time-reversed mating call (r*) (f) were first presented in silence (SNR ∞). Next an increasing pink noise background was added (SNR decreasing from 6 to –6 dB).

Further explanation in text.

an increasing background of pink noise. The response to the mating calls decreases with decreasing signal-to-noise ratio (SNR) whereas there is practically no response to the time-reversed mating calls. The SNR is defined here as the peak ratio between the vocalizations and the noise. There is no response to the pink noise, which is indicated by the empty lines between r* and * in Fig. 4f. Other units with similar response characteristics were also found, see Table I in Van Stokkum (1987).

There are several possible ways to model the

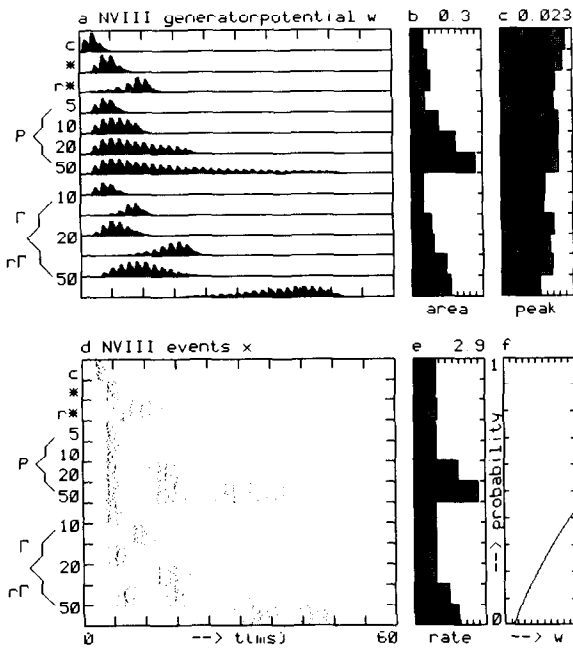


Fig. 5. Output of a model simulation of a NVIII fibre showing the timecourse of the generator potential w (a), its area (b) and its peak (c) as a function of pulse shape. Stimulus parameters: intensity -20 dB relative to q^0 , carrier frequency 0.625 kHz. Tuning: F_c 0.625 kHz, β 1.0 ms, amphibian papilla. The reordered event display (d) and rate histogram (e) of the NVIII events x are produced with help of the probability of event generation shown in Fig. 5f. Parameters for the event generation: m 0.003 , binwidth 0.1 ms. A delay of 2 ms was incorporated. Refractory parameter: τ_{abs} 5 ms. Other parameters in Table I.

preference for fast intensity changes. To model the transient response to the AM tonebursts (Figs. 4c and 4d) we take brief short-term adaptation in combination with slow recovery, to achieve strong adaptation.

In Figs. 5a-c and 6a-c the effect of this strong adaptation on the generator potential w is shown. The generator potential shown in Figs. 5a and 6a is calculated excluding the negative feedback provided by the refractory mechanism (Fig. 1G). Each row shows w as a function of the time indicated at the bottom and belonging to the stimulus indicated at the left. The histograms of Figs. 5b and 5c depict the area under and the peak of the generator potential, belonging to a row in Fig. 5a. With the pulse shape variations the generator potential shows a greater peak and a smaller area for the normal versus the time-reversed shapes

(Figs. 5 a-c). With the AM tonebursts (Fig. 6a) a transient response character is visible: the peak of w is reached between 50 and 100 ms after the onset, thereafter the response declines. The peak of the generator potential (Fig. 6c) shows a broad maximum for intermediate AMFs.

The next step is to consider the generation of action potentials. In this model the event generator plays a central role, and it is important to visualize the probability of event generation, according to Eq. 12. Figs. 5f and 6f show this probability as function of the generator potential w , drawn for the potential range of, respectively, Figs. 5c and 6c. The rate response of the NVIII model neuron is non-selective with regard to pulse shape (Figs. 5d and 5e) and shows a weakly band-pass character with regard to AMF (Figs. 6d and 6e). Furthermore, the response to the AM tonebursts, Fig. 6d, shows the desired transient character.

Now we model the convergence of NVIII fibres upon a DMN neuron. We slightly vary the thresholds of 16 NVIII fibres and their absolute refractory periods, to achieve a range of response

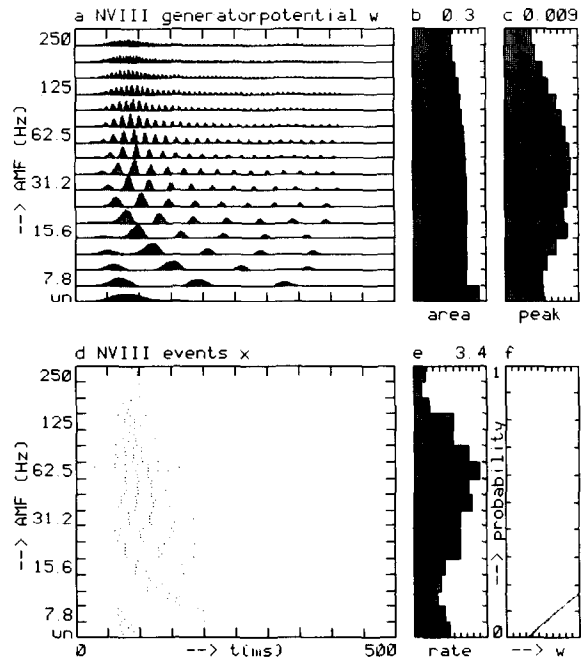


Fig. 6. Simulation of a NVIII fibre. Outputs w , the generator potential, and x , the events, as a function of AMF. Format and parameters as in Fig. 5.

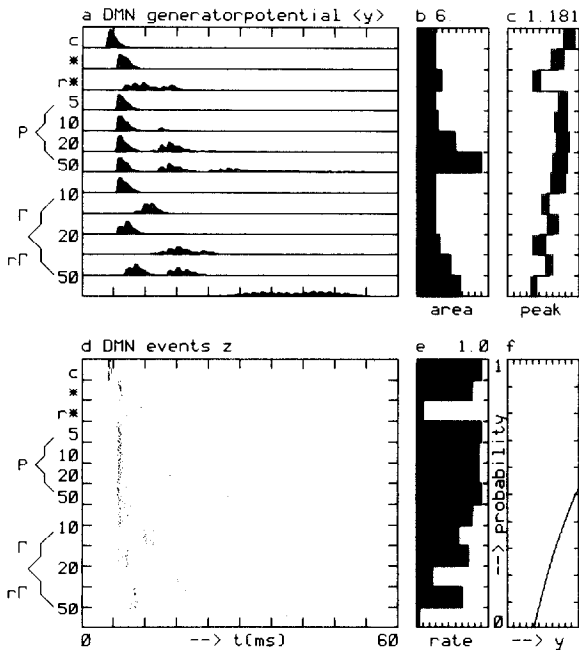


Fig. 7. Simulation of a DMN neuron. Outputs y , the generator potential, and z , the events, as a function of pulse shape. In contrast with Fig. 5 the timecourse of the ensemble averaged generator potential $\langle y(t) \rangle$ (a), its area (b) and the average and standard deviation of the peak of $y(t)$ (c) are depicted. Inputs are 16 units, with m varying linearly between 0.0003 and 0.003, and τ_{abs} between 4 and 5 ms. The values of 0.003 for m and 5 ms for τ_{abs} were used in Figs. 5 and 6.

patterns (see legend Fig. 7). These NVIII fibres will demonstrate a large amount of synchrony in their responses to fast intensity changes, but will respond more asynchronously to slow intensity changes. Convergence of these fibres upon a DMN unit will result in a peaked generator potential for the DMN unit in case of synchronous inputs, and in a smaller but more prolonged generator potential in case of asynchronous inputs. The threshold of the DMN unit is adjusted to the height of several EPSPs. So the second mechanism (the first being adaptation) to favour the fast intensity changes is to take a number of NVIII units with slightly different characteristics, and model the DMN unit as a coincidence detector. The effect of the coincidence detection is expected to grow along with the number of different inputs.

The characteristics of the DMN generator potential y are illustrated in Figs. 7a-c and 8a-c, where as before refractory effects have been

excluded. In Fig. 7a we have averaged $y(t)$ over the 20 presentations of the stimulus, resulting in an ensemble average $\langle y(t) \rangle$. In Fig. 7c the average peak of $y(t)$ is drawn, which is not equal to the peak of $\langle y(t) \rangle$. The deviations from the solid line in Fig. 7c indicate the standard deviation of the peak of $y(t)$.

Comparing Figs. 5a and 7a we note the following differences: the periodicity in Fig. 5a, which was the result of phaselocking, has almost disappeared in Fig. 7a. This is due to the smoothing by the EPSP, the convergence of the 16 inputs, and to the ensemble averaging. The average peak of y is higher for all normal versus time-reversed shapes (Fig. 7c). This difference is still larger for the peak of $\langle y(t) \rangle$ in Fig. 7a. Figs. 8a and 8c show a larger peak for AMF's around 50 Hz, the difference again being larger in Fig. 8a. Using the probabilities of event generation shown in Figs. 7f and 8f we now obtain selective responses, which resemble those of Figs. 4a and 4c qualitatively. The rate histogram in Fig. 7e shows a decreased response to the time-reversed stimuli r^* , $r\Gamma 20$ and $r\Gamma 50$. Furthermore, the response to the stimuli with short

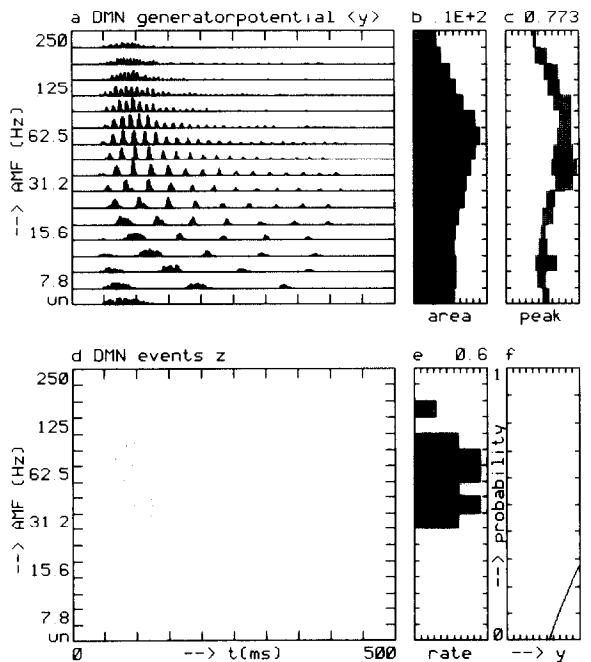


Fig. 8. Simulation of a DMN neuron. Outputs y , the generator potential, and z , the events, as a function of AMF. Format and parameters as in Fig. 7.

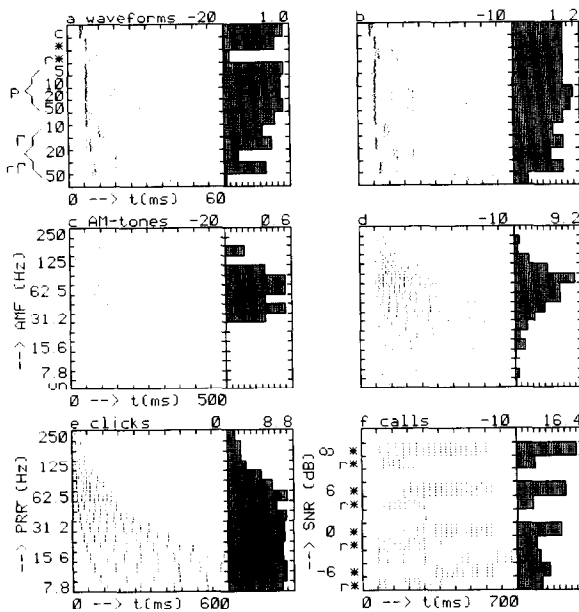


Fig. 9. Reordered event displays together with rate histograms of the model DMN neuron of Figs. 7 and 8 in response to the six stimuli of Fig. 4. (a) and (c) are equal to, respectively, Figs. 7d-e and 8d-e. All stimuli are presented at the relative intensities of Fig. 4. The intensities in dB relative to q^0 are indicated above each eventdisplay.

rise times is very precisely timed (Fig. 7d). The response to the AM tonebursts (Figs. 8d and 8e) shows a band-pass character with respect to AMF.

The responses of this DMN model neuron to all of the stimuli of Fig. 4 are shown in Fig. 9. The parameters were adjusted in order to achieve a qualitative resemblance to the responses to all six different stimuli of Fig. 4. Comparing Figs. 4 and 9 we note the following deviations: the response in Fig. 4b is restricted to the onset, in Fig. 4d the response is more transient, and the rate response to the click trains (Fig. 4e) is larger. The time-reversed mating calls (r^*) and the noise evoke practically no response (Fig. 4f). Enhancement of the transient character of the model's response by means of stronger adaptation will decrease the response to the click trains, which already suffers from the adaptation. Nevertheless the response of this model (Fig. 9) qualitatively resembles the real data in Fig. 4. We have found other DMN neurons which showed responses more like Figs. 9b and 9d, see e.g. Fig. 6b in Van Stokkum (1987).

Not shown here are the responses to tonepips

with varying carrier frequency. The model generates onset events between 0.4 and 0.8 kHz at -20 dB relative to q^0 and between 0.2 and 1.0 kHz at -10 dB. This deviates only slightly from the onset response of unit 297,0,6 to tonepips with carrier frequencies between 0.5 and 0.8 kHz at 80 dB and between 0.4 and 1.1 kHz at 90 dB.

Recently, Hall and Feng (1988a) investigated phasic neurons in the DMN of the leopard frog (*Rana p. pipiens*). In accordance with the findings of Van Stokkum (1987) in the grassfrog (*Rana temporaria*), they also found a preference for rapid rise times. Their stimulus consisted of tonepips at CF with a duration of 300 ms and a linear rise time varying between 1 and 100 ms. At 10 dB above threshold most phasic neurons did not respond to tonepips with rise times larger than 25 ms, just like our unit 297,0,6 did not respond to $r\Gamma 50$ (Figs. 4a and 4b) which has a rise time of 40 ms. Hall and Feng systematically investigated the rate and latency as a function of rise time, at several intensities. We presented their stimuli to our model with the same parameters as in Figs. 5–9.

The simulated NVIII fibre (Figs. 10a and 10b) responds only to rise times shorter than 25 ms at an intensity of -30 dB relative to q^0 (\times). At an intensity of -20 dB (\diamond) and above the rate response is non-selective, in accordance with Fig. 5e. The latency characteristics in Fig. 10b show large slopes at the lowest intensities (\times : 0.75, \diamond : 0.35) and are nearly flat at the highest intensities (\triangle : 0.1, \square : 0.05). The simulated DMN neuron responds preferentially to the rapid rise times at intensities between -30 and -10 dB (Fig. 10c). This is in accordance with the responses shown in Figs. 9a and 9b, and also corresponds well with Fig. 3 in Hall and Feng (1988a). The latency characteristics in Fig. 10d show larger slopes than in Fig. 10b. In accordance with the findings of Hall and Feng, the slope decreases when the intensity is increased from -20 to 0 dB (\diamond : 0.6, \square : 0.15).

Discussion

The aim of our study was to model the response characteristics of NVIII fibres and DMN neurons by incorporating several data from the

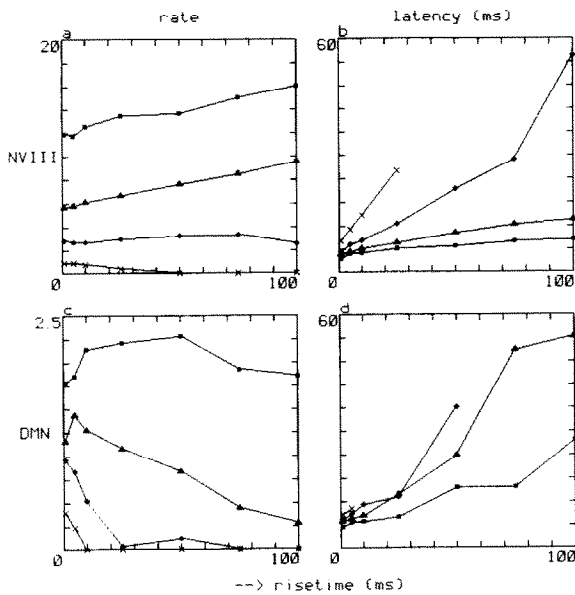


Fig. 10. Response of the NVIII (a,b) and of the DMN neuron (c,d) simulated in Figs. 5–9 to tonepips at CF with varying rise time, following the paradigm of Hall and Feng (1988a). The intensity, in dB relative to q^0 , is indicated by symbols: -30 (\times), -20 (\diamond), -10 (\triangle), 0 (\square). All data points are averages over 25 stimulus presentations. The rate response is measured in spikes per stimulus presentation.

literature on isolated parts of the peripheral auditory system into a coherent model. We conclude that the model was successful in reproducing the general behavior of NVIII fibres and DMN neurons. In particular, by varying the adaptation parameters and the amount of coincidence detection we obtained the different temporal selectivities found in the NVIII and in the DMN. To arrive at a parameter set which reproduces all of the response characteristics of a single neuron in detail is a time consuming trial and error procedure. In our view, the main result of this study is that the responses of different neurons in the NVIII and DMN to a wide set of stimuli can be modeled adequately with a single set of parameters for each single neuron.

Model simulations

The main deviations between Figs. 4 and 9 arise with spectrally broader stimuli like clicks, mating calls and noise. In our model we have assumed that the NVIII units which converged

upon the DMN unit all had the same spectral characteristics. When we also allow the centre frequencies of the input units to vary a little, an improvement is expected of the responses to fast intensity changes. Fast intensity changes are spectrally broad, and thus are expected to excite a larger number of inputs with slightly different spectral characteristics. In contrast, tonal stimuli are spectrally narrow and will excite a relatively smaller number of inputs.

The responses of the real neuron were more transient than those of the model neuron, compare Figs. 4b,d with Figs. 9b,d. We expect a more transient response of the model neuron when we include adaptation in the synapses between NVIII fibres and DMN neuron. This can be modeled with a long τ_R of the DMN neuron (see also Bibikov and Ivanitskii, 1985).

It was shown in Fig. 10 that our model also reproduces the rate and latency characteristics of Hall and Feng (1988a). They concluded that the phasic DMN neurons behaved as low-pass temporal filters with respect to envelope rise time. We prefer to interpret the selectivity for rapid rise times as a preference for fast intensity changes. Our simulations show that at intensities more than 30 dB above threshold the preference for rapid rise times has vanished (Fig. 10c). At these high intensities even the onset of a tonepip with a rise time of 100 ms corresponds with a large increment in absolute intensity, relative to the preceding silence. The simulations of the NVIII fibre in Figs. 10a and 10b predict that the phasic NVIII fibres also prefer fast intensity changes at stimulus intensities just above threshold.

There remains a fundamental problem with the evaluation of the model's output, since it is an unsolved problem how event trains with a stochastic character should be compared quantitatively (Aertsen et al., 1979). How can we measure the difference between, say, the responses shown in Figs. 4a and 9a? Qualitatively we may look for global differences, such as the presence or absence of selectivity, see e.g. the lack of response to $r\Gamma 50$. In this study we have used averages of the response, such as rate or mean and standard deviation of the latency. We have presented reordered eventdisplays, which form a complete representation of the data, and rate histograms. Comparing

Figs. 4d and 9d we immediately note, next to the global resemblance, the differences in the transient character of the response and in the degree of AMF selectivity.

Frequency tuning

With regard to the spectral filtering it is clear that the model is rather crude, and has some simplifying assumptions. We want to discuss the following points:

We have assumed linearity of the middle ear, which is only justified up to 1.5 kHz (Vlaming et al., 1984).

We have chosen the effective stimulus for the haircells to be the sound pressure displacement. Choosing the velocity, i.e. its derivative, will produce a gain of 6 dB per octave in the middle-ear transfer function at the bottom of Fig. 2. The tuning curve of the low-frequency unit of Fig. 2 will then be broadened.

The two different parallel sequences, nonlinearity followed by band-pass filter (Figs. 1B,C) and vice-versa (Figs. 1D,E), are two extremes. In addition to the band-pass filter and the static nonlinearity the membrane of the basilar papilla haircell performs a low-pass filtering action. This is not incorporated in the model.

The nonlinear phenomenon of two-tone suppression has only been observed in fibres with characteristic frequencies (CFs) below 0.5 kHz. Fibres innervating the amphibian papilla with CF between 0.5 and 1.0 kHz do not show two-tone suppression. This suggests two stages of filtering in the amphibian papilla: a mechanical stage which is perhaps related to the travelling wave suggested by Hillery and Narins (1984), and an active electrical tuning of the haircell membrane. The mechanical filtering in the amphibian papilla would then prevent two-tone suppression in haircells tuned to frequencies between 0.5 and 1.0 kHz.

In summary, both papillae should be modeled with a band-pass filter followed by a nonlinear mechano-electrical transduction. In the amphibian papilla the haircell membrane probably represents a band-pass filter, whereas in the basilar papilla it performs a low-pass filtering action. In our model we have chosen the two extremes to

demonstrate the sequence effect, and because of simplicity.

We have made no attempt to model active tuning of the amphibian papilla. This is expected to improve the frequency tuning, but would require the introduction of additional nonlinearities. Lewis (1988), in discussing the fundamental problems which arise in modeling bidirectional active processes, pointed at the need of considering the amphibian papilla as a whole.

We have disregarded the dynamical aspects of the mechano-electrical transduction. This is a simplification, since Corey and Hudspeth (1983) found that the time-constants involved are on the order of 0.1 ms, which is not instantaneous with respect to filter time-constants.

Coincidence detection

The main mechanisms which appear to contribute to temporal selectivity are short-term adaptation, event generation and coincidence detection. Coincidence detection has also been suggested by Kim et al. (1986) to explain the 'pitch-period following response' found in neurons of the posteroventral cochlear nucleus in cats. These neurons responded to the fast intensity changes in speech like sounds. The coincidence detection is of course critically dependent upon the EPSP shape and the number of inputs. A longer EPSP duration results in more temporal integration, and favours the stimuli which produce more events in NVIII. This deteriorates the selectivity for fast intensity changes, as developed with this model. It has been shown by Bibikov and Kalinkina (1983) that DMN neurons integrate the stimulus energy over a range of 2 to 5 ms. This supports our choice of 1 ms for the EPSP decay time-constant.

With regard to the number of inputs, we also tried convergence of two, four and eight NVIII fibres upon a DMN unit. The preference for fast intensity changes was already present with four inputs, albeit weaker. Thus far we have not allowed for intranuclear inhibition, because this has not yet been demonstrated in the anuran DMN.

Parameter variation

Finally we summarize the significance of the parameters of Table I. A first group of parameters

(γ , ω_1 , ρ , q^0 , r^0 , ω_i , β_i , u_0 , λ , μ , ω_2) is responsible for the NVIII generator potential w . Variation of ω_i and β_i produces different spectral selectivities (Fig. 2). Variation of the adaptation parameters λ and μ produces the different types of short-term adaptation found in the NVIII by Megela and Capranica (1981, 1982) (Fig. 3).

The neuronal refractory (τ_{abs} , R , τ_{R}) and event generation (ν , m) properties have to be adjusted to produce realistic response properties. Thereby τ_{abs} is chosen equal to the neuron's smallest interspike interval. Presumably the pauser neurons recently reported by Hall and Feng (1988b) can be modelled with an appropriate choice of the refractory parameters. The threshold m was responsible for the response selectivity derived from the generator potential.

The amount of spatiotemporal integration is responsible for the developed selectivity for temporal characteristics of sound. The response with one NVIII input will resemble that input. Thereby temporal integration may decrease the phase-locking ability. The response to a larger number of NVIII inputs may show coincidence detection as discussed above. The degree of coincidence detection grows with increasing m and n , and with decreasing τ_d and τ_u .

We conclude that detailed neural modeling contributes to the appreciation of neural data. In particular the use of one set of parameters to reproduce the response characteristics of a single neuron to a broad ensemble of stimuli results in a functional description of the neuron.

Acknowledgements

This investigation was supported by the Netherlands Organization for Scientific Research (NWO). The authors thank Willem Epping and Peter Johannesma for insisting on systematic modeling of the auditory periphery and Willem Melssen for software assistance. Furthermore all three are thanked for helpful discussions and critical reading of the text.

References

Aertsen, A.M.H.J. and Johannesma, P.I.M. (1980) Spectrotemporal receptive fields of auditory neurons in the grass-

- frog. I. Characterization of tonal and natural stimuli. *Biol. Cybern.* 38, 223–234.
- Aertsen, A.M.H.J., Smolders, J.W.T. and Johannesma, P.I.M. (1979) Neural representation of the acoustic biotope: on the existence of stimulus-event relations for sensory neurons. *Biol. Cybern.* 32, 175–185.
- Aertsen, A.M.H.J., Vlaming, M.S.M.G., Eggermont, J.J. and Johannesma, P.I.M. (1986) Directional hearing in the grassfrog (*Rana temporaria* L.): II. Acoustics and modelling of the auditory periphery. *Hear. Res.* 21, 17–40.
- Bibikov, N.G. and Kalinkina, T.V. (1983) Properties of the acoustic neurons of the dorsal medullary nucleus in *Rana ridibunda*. *J. Evol. Biochem. Physiol.* 18, 346–352.
- Bibikov, N.G. and Ivanitskii, G.A. (1985) Modelling spontaneous pulsation and short-term adaptation in the fibres of the auditory nerve. *Biophysics* 30, 152–156.
- Capranica, R.R. and Moffat, A.J.M. (1980) Nonlinear properties of the peripheral auditory system of anurans. In: A. Popper and R. Fay (Eds.), *Comparative studies of hearing in vertebrates*, Springer, New York, pp. 139–165.
- Corey, D.P. and Hudspeth, A.J. (1983) Kinetics of the receptor current in bullfrog saccular hair cells. *J. Neurosci.* 5, 962–976.
- Cox, D.R. and Isham, V. (1980) *Point processes*. Chapman and Hall, London.
- Crawford, A.C. and Fettiplace, R. (1980) The frequency selectivity of auditory nerve fibres and hair cells in the cochlea of the turtle. *J. Physiol.* 306, 79–125.
- Crawford, A.C. and Fettiplace, R. (1981a) An electrical tuning mechanism in turtle cochlear hair cells. *J. Physiol.* 312, 377–412.
- Crawford, A.C. and Fettiplace, R. (1981b) Non-linearities in the responses of turtle hair cells. *J. Physiol.* 315, 317–338.
- De Boer, E. and Kuypers, P. (1968) Triggered correlation. *IEEE Trans. Biomed. Eng.* 15, 169–179.
- Eggermont, J.J. (1985) Peripheral auditory adaptation and fatigue: A model oriented review. *Hear. Res.* 18, 57–71.
- Epping, W.J.M. and Eggermont, J.J. (1986) Sensitivity of neurons in the auditory midbrain of the grassfrog to temporal characteristics of sound. II. Stimulation with amplitude modulated sound. *Hear. Res.* 24, 55–72.
- Feng, A.S. (1982) Quantitative analysis of intensity-rate and intensity-latency functions in peripheral auditory nerve fibers of northern leopard frogs (*Rana p. pipiens*). *Hear. Res.* 6, 241–246.
- Feng, A.S. (1986) Afferent and efferent innervation patterns of the cochlear nucleus (dorsal medullary nucleus) of the leopard frog. *Brain Res.* 367, 183–191.
- Fritzsche, B., Ryan, M.J., Wilczynski, W., Hetherington, T.E. and Walkowiak, W. (Eds.) (1988) *The Evolution of the Amphibian Auditory System*. Wiley, New York.
- Gerhardt, H.C. and Doherty, J.A. (1988) Acoustic communication in the green treefrog, *Hyla versicolor*: evolutionary and neurobiological implications. *J. Comp. Physiol. A* 162, 261–278.
- Hall, J.C. and Feng, A.S. (1988a) Influence of envelope rise time on neural responses in the auditory system of anurans. *Hear. Res.* 36, 261–276.

- Hall, J.C. and Feng, A.S. (1988b) Response properties of single auditory neurons in the dorsal medullary nucleus of the frog. *Soc. Neurosci. Abstr.* 14, 649.
- Hillery, C.M. and Narins, P.M. (1984) Neurophysiological evidence for a traveling wave in the amphibian inner ear. *Science* 225, 1037–1039.
- Hillery, C.M. (1984) Detection of amplitude-modulated tones by frogs: Implications for temporal processing mechanisms. *Hear. Res.* 14, 129–143.
- Hillery, C.M. and Narins, P.M. (1987) Frequency and time domain comparison of low-frequency auditory nerve fiber responses in two anuran amphibians. *Hear. Res.* 25, 233–248.
- Hudspeth, A.J. (1983) Transduction and tuning by vertebrate hair cells. *Trends Neurosci.* 6, 366–369.
- Johannesma, P.I.M. (1971) Dynamical aspects of the transmission of stochastic neural signals. In: E. Broda, A. Locker, H. Springer-Lederer (Eds.), *First European biophysics congress*, Verlag der Wiener medizinischen akademie, Vienna, pp. 329–333.
- Johannesma, P.I.M. and Van den Boogaard, H.F.P. (1985) Stochastic formulation of neural interaction. *Acta Applic. Math.* 4, 201–224.
- Kim, D.O., Rhode, W.S. and Greenberg, S.R. (1986) Responses of cochlear nucleus neurons to speech signals: neural encoding of pitch, intensity and other parameters. In: B.C.J. Moore and R.D. Patterson (Eds.), *Auditory Frequency Selectivity*, Plenum, New York, pp. 39–48.
- Lewis, E.R. (1988) Tuning in the bullfrog ear. *Biophys. J.* 53, 441–447.
- Meddis, R. (1986) Simulation of mechanical to neural transduction in the auditory receptor. *J. Acoust. Soc. Am.* 79, 702–711.
- Mégela, A.L. (1984) Diversity of adaptation patterns in responses of eighth nerve fibers in the bullfrog, *Rana catesbeiana*. *J. Acoust. Soc. Am.* 75, 1155–1162.
- Mégela, A.L. and Capranica, R.R. (1981) Response patterns to tone bursts in peripheral auditory system of anurans. *J. Neurophysiol.* 46, 465–478.
- Mégela, A.L. and Capranica, R.R. (1982) Differential patterns of physiological masking in the anuran auditory nerve. *J. Acoust. Soc. Am.* 71, 641–645.
- Palmer, A.R. and Russell, I.J. (1986) Phase-locking in the cochlear nerve of the guinea-pig and its relation to the receptor potential of inner hair-cells. *Hear. Res.* 24, 1–15.
- Pitchford, S. and Ashmore, J.F. (1987) An electrical resonance in hair cells of the amphibian papilla of the frog *Rana temporaria*. *Hear. Res.* 27, 75–83.
- Rall, W. (1977) Core conductor theory and cable properties of neurones. In: *Handbook of Physiology, Sect. 1: The nervous system, Vol. I: Cellular biology of neurons, part 1*, American Physiological Society, Bethesda, MD, pp. 39–97.
- Schneider-Lowitz, B. (1983) *Neuronaler Verarbeitung einfacher und komplexer Schallsignale in der Peripherie und den unteren Stationen der Hörbahn des Grasfrosches (Rana t. temporaria L.)*. Thesis, Bonn, F.R.G.
- Vlaming, M.S.M.G., Aertsen, A.M.H.J. and Epping, W.J.M. (1984) Directional hearing in the grassfrog (*Rana temporaria* L.): I. Mechanical vibrations of the tympanic membrane. *Hear. Res.* 14, 191–201.
- Van Gisbergen, J.A.M., Grashuis, J.L., Johannesma, P.I.M. and Vendrik, A.J.H. (1975) Neurons in the cochlear nucleus investigated with tone and noise stimuli. *Exp. Brain Res.* 23, 387–406.
- Van Stokkum, I.H.M. (1987) Sensitivity of neurons in the dorsal medullary nucleus of the grassfrog to spectral and temporal characteristics of sound. *Hear. Res.* 29, 223–235.
- Whitehead, M.L., Wilson, J.P. and Baker, R.J. (1986) The effects of temperature on otoacoustic emission tuning properties. In: B.C.J. Moore and R.D. Patterson (Eds.), *Auditory Frequency Selectivity*, Plenum, New York, pp. 39–48.
- Zakon, H.H. and Wilczynski, W. (1988) The physiology of the anuran eighth nerve. In: B. Fritzsche et al. (Eds.), *The Evolution of the Amphibian Auditory System*, Wiley, New York, pp. 125–155.